Tailorable Multi-Modular Pore-Space-Partitioned Vanadium Metal-Organic Frameworks for Gas Separation

Wei Wang,[a] Yichong Chen,[b] Pingyun Feng[b], and Xianhui Bu*[a]*

Wei Wang, Xianhui Bu

Department of Chemistry and Biochemistry, California State University Long Beach, Long Beach, CA 90840, United States

E-mail: xianhui.bu@csulb.edu

Yichong Chen, Pingyun Feng

Department of Chemistry, University of California, Riverside, Riverside, CA 92521, United States

E-mail: pingyun.feng@ucr.edu

Keywords: vanadium, metal-organic framework, multi-module, pore space partition, gas separation

Currently, few porous vanadium metal-organic frameworks (V-MOFs) are known and even fewer are obtainable as single crystals, resulting in limited information on their structures and properties. Here we demonstrate remarkable promise of V-MOFs by presenting an extensible family of V-MOFs with tailorable pore geometry and properties. The synthesis leverages inter-modular synergy on a tri-modular pore-partitioned platform. New V-MOFs show a broad range of structural features and sorption properties suitable for gas storage and separation applications for C_2H_2/CO_2, C_2H_6/C_2H_4, and C_3H_8/C_3H_6. The *c*/*a* ratio of the hexagonal cell, a measure of pore shape, is tunable from 0.612 to1.258. Other tunable properties include pore size from 5.0 to 10.9 Å and surface area from 820 to 2964 $m^2\ g^{-1}$. With C_2H_2/CO_2 selectivity from 3.3 to 11 and high uptake capacity for C_2H_2 from 65.2 to 182 $cm^3\ g^{-1}$ (298K, 1 bar), an efficient separation is confirmed by breakthrough experiments. The near-record high uptake for C_2H_6 (166.8 $cm^3\ g^{-1}$) contributes to the promise for C_2H_6-selective separation of C_2H_6/C_2H_4. The multi-module pore expansion enables transition from C_3H_6-selective to more desirable C_3H_8-selective separation with extraordinarily high C_3H_8 uptake (254.9 $cm^3\ g^{-1}$) and high separation potential (1.25 mmol g^{-1}) for C_3H_8/C_3H_6 (50:50 v/v) mixture.

1. Introduction

To researchers accustomed to metal-organic framework (MOF) materials based on prevalent divalent metals (e.g., Mg, Mn-Zn, Cd),[1-3] MOFs with high-valent (> +2) metals (e.g., Al/Ga/In, Sc/Y/Ln, Ti/Zr, V, Cr) have always been a source of inspiration.[4-7] Due to significant differences between these metals in fundamental characteristics such as ionic radii, oxidation states, and electron configurations (and resulting differences in Pearson hardness parameter, solvolysis and condensation behaviors, redox properties), MOF chemistry of these higher-valent metal ions differs significantly from one another and therefore each of these MOF compositions needs to be approached with an individualized approach (especially in their synthesis), making the development of high-valent MOFs a fascinating journey.[8] In this work, encouraged by our past successes with high-valent indium[9] and chromium[10] MOFs, we seek to tackle some synthetic challenges in other high-valent compositions.

Among high-valent MOFs, vanadium MOF (V-MOF) stands out as one of the most difficult to develop. This apparent difficulty came to light in several aspects after a literature study. Firstly, even though more than two decades have passed since the report of the first V-MOF (MIL-47) in 2002,[11] so far only about ten V-MOFs have been reported with permanent porosity. These porous V-MOFs consist of VO-chain-type MIL-47, MIL-68,[12] MIL-71,[13] MOF-48,[14] MFM-300,[15] NU-2001[16] and V_3O-trimer-type MIL-100,[17] MIL-101,[18] BIT-66.[19] These V-MOFs all have structures (including ligands used) that are the same as those based on other metals such as Al, Cr, and In.[20-23]

Secondly, an examination of V-MOF literature also reveals the apparent difficulty in growing X-ray-quality single crystals, which takes away many advantages single crystals can offer. Clearly, the difficulty in growing single crystals suitable for conventional X-ray diffraction would impede the development of any new crystalline platform. Unlike Cr-MOFs which are difficult to grow large crystals due to kinetic inertness of Cr^{3+}, V-MOFs are not subject to such limitation so that other factors impacting crystal growth need to be probed. These factors include solvent type, reaction temperature and time, whose choices should be reconciled with the need to avoid unwanted products such as discrete clusters. The vanadium system is particularly prone to deviate from intended products, in part due to multiple stable oxidation states (+3, +4, +5), which is not usually a problem for other MOF metals such as indium and chromium. The results from the literature indicate that V-O chain-based V-MOFs can be grown into single crystals by using higher-than-normal MOF-synthesis-temperatures (≥ 200 °C), but this high-temperature approach is less desirable in terms of porosity generation and control. So

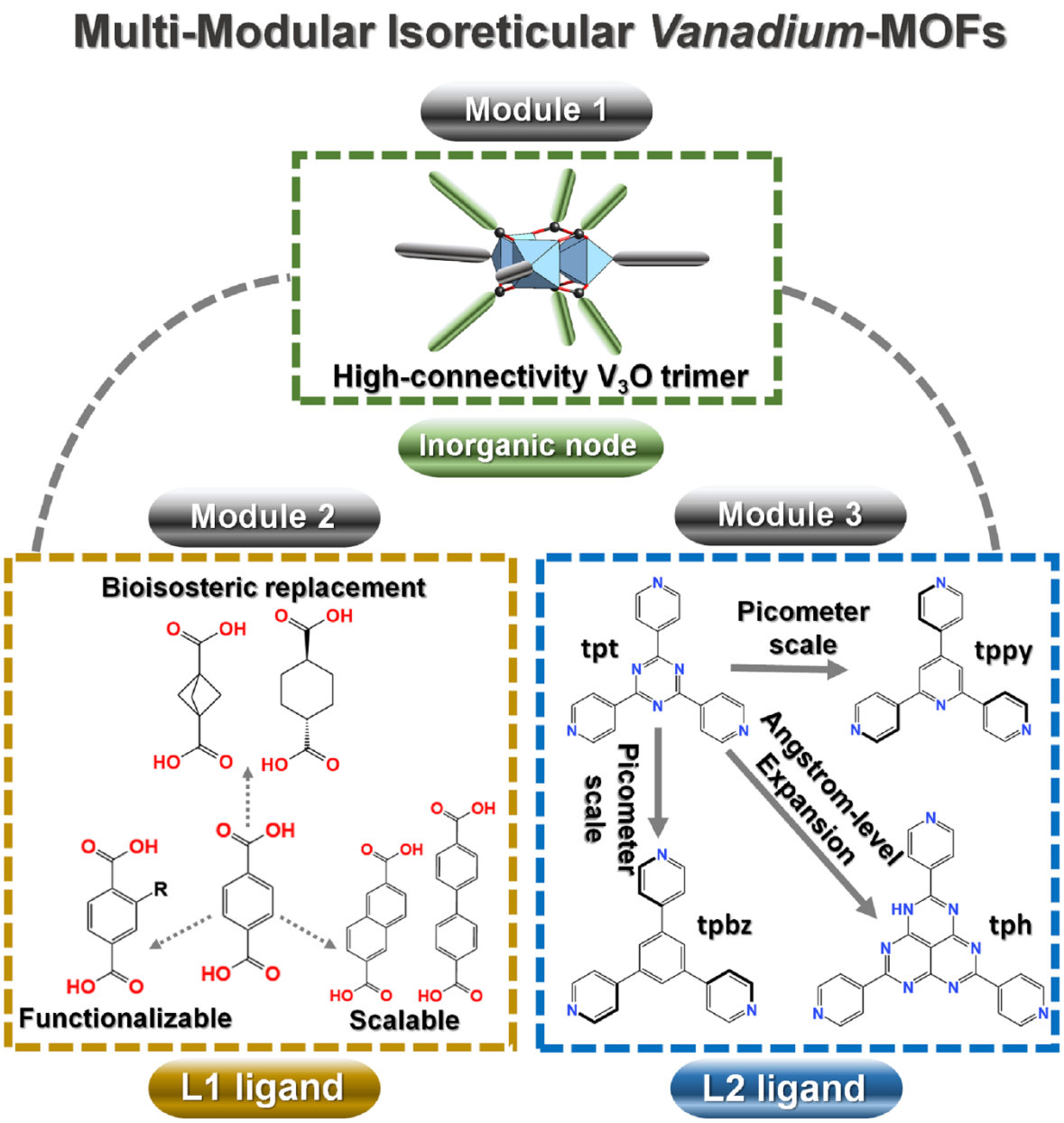

Scheme 1. Illustration of a highly expansible multi-modular isoreticular vanadium-MOF system using the prototypical V-bdc-tpt as the starting point for isoreticular replacement. The picometer-scale change from tpt to tppy and tpbz originates from the difference between C-C and C-N bond lengths. L1: bdc = terephthalic acid, abdc = 2-amino-1,4-benzenedicarboxylic acid, Brbdc = 2-bromo-1,4-benzenedicarboxylic acid, bcp = bicyclo[1.1.1]pentane-1,3-dicarboxylic acid, chdc = *trans*-1,4-cyclohexanedicarboxylic acid, 26ndc = 2,6-naphthalenedicarboxylic acid, bpdc = 4,4'-biphenyldicarboxylic acid, L2: tpt = 2,4,6-tri(4-pyridyl)-1,3,5-triazine, tppy = 2,4,6-tri(4-pyridyl)pyridine, tpbz = 1,3,5-tri(4-pyridyl)benzene, tph = 2,5,8-tri-(4-pyridyl)-1,3,4,6,7,9-hexaazaphenalene.

far, the single-crystal growth of trimer-based V-MOFs (e.g., MIL-88-V, MIL-100-V, MIL-101-V, BIT-66) remains a challenge.[17-19] In fact, we are not aware of any porous trimer-based V-MOFs that were characterized by single crystal X-ray diffraction (trimer-containing MIL-59 single crystals are non-porous).[24]

Finally, further hampering the development and potential applications of V-MOFs is the observation that the reported V-MOFs show a nearly complete lack of isoreticular chemistry which is the tuning of porosity and other properties through component substitutions (e.g., scaling of ligand geometry) on the same topological platform. Such inability to tune a MOF platform isoreticularly makes it difficult to optimize their pore properties to target specific applications.

The work reported here represents a dramatic advance in addressing all aforementioned limitations of known V-MOFs (i.e., the low number of known porous V-MOFs, the powder dilemma, lack of isoreticular chemistry and pore tailorability). The number of new porous V-MOFs from this work is comparable to the cumulative total of all porous V-MOFs made in the past two decades.[7, 25] In addition to the optimization of synthesis conditions, a key to the success of this work is the use of a multi-module MOF platform called *pacs* (partitioned *acs*) which represents a total departure from the past approach used in V-MOFs.[26] A module is a part of the structure with a specific structural role or function. For example, module 3 in *pacs* (Scheme 1) is mainly responsible for the pore space partition and framework stabilization. A module can be as simple as a metal ion (e.g., Ag^+ in CPM-550) or a single organic ligand (e.g., tpt), but can also be very complex with multiple metal ions and multiple ligands (e.g., in CPM-32, CPM-400, and CPM-500).[27-28] An analysis of known V-MOFs shows that they all have simple chemical compositions with the framework made of just two modules (i.e., one inorganic node and one type of crosslinking ligand). The limited success with V-MOFs in such two-module systems points to a need to go beyond simple two-module systems and to investigate more complex chemical compositions.

Multi-module systems can offer a number of advantages including far more diverse isoreticular chemistry and the ability to tune pore properties independently along different crystallographic directions. Here, the multi-modularity of the *pacs* platform comes from a design concept called pore space partition (PSP). To apply PSP strategy, another module (a pore-partitioning unit) is implanted covalently to divide large-cage or continuous-channel pore space into smaller pieces. The trimer-based *pacs*-type MOF has general formula of $[M_3(O/OH)(L1)_3(L2)]$, where L1 is a ditopic ligand for forming the *acs* net (MIL-88/MOF-235),[29-30] and L2 is a pore-partitioning ligand which is an identifying feature of the *pacs*

platform. The doping of vanadium into the *pacs* system in the form of Mg_2V,[31] Co_2V,[32] and Ni_2V[33] has contributed to the dramatic enhancement of gas uptake and separation properties. However, trimers based on mixed metals can be very different from those based on one metal type in many aspects including the level of difficulty in synthesis. This is actually the case for vanadium (also Al, Cr etc.). The fact is that pure-vanadium-based *pacs* materials have evaded many synthetic attempts until this work.

Crystallization-based materials' discovery processes involving multi-module systems can be unpredictable and frustrating due to various traps with less desirable phases. However, properly designed multi-module systems with built-in complementary features can generate synergistic structure-direction effects that suppress less desirable phases (often containing fewer modules) as well as provide a strong driving force for multi-component co-assembly towards target multi-module products. For example, on the *pacs* platform,[9, 26-28, 31-49] both L1 and L2 ligands are capable of inducing the trimer formation as well as stabilizing the trimer. In comparison, on the MIL-88 (*acs*) platform,[29] only L1 ligand can help with the stabilization of trimer (the stabilizing effect by coordinating solvent molecules in MIL-88 is far weaker than pore-partition L2 ligand in *pacs*). This difference between dual-ligand control and one-ligand control can be greatly magnified when the inorganic unit is less stable due to competing reactions, as is the case for vanadium which has a pronounced tendency to form vanadyl species and related clusters (e.g., polyoxovanadate) with low- to zero-connectivity.

Here we report a large and extensible family of V-MOFs (collectively called V-*pacs*). These materials are stable for gas separation applications as confirmed by multiple cycles of breakthrough experiments. We demonstrate their impressive gas sorption properties for possible separation applications for three industrially important gas pairs, C_2H_2/CO_2, C_2H_6/C_2H_4, and C_3H_8/C_3H_6. These V-MOFs were synthesized from seven types of L1 ligands and four types of L2 ligands. So far, 14 V-MOFs have been made and they are the first high-connected (> 6) V-MOFs which are beneficial for achieving greater stability. Previous V-MOFs are based on 4-connected VO chain-type structures or 6-connected V_3O trimers. The new V-MOFs are also the first trimer-based porous V-MOFs grown into X-ray-quality single crystals which provide much greater clarity into structural details and offer promise for advanced characterizations such as the study of host-guest chemistry including determination of guest molecule locations in adsorption and separation applications.

In this work, 14 new V-*pacs* materials obtained through various combinations between L1 and L2 ligands are denoted using the names of their three separate modules as follows: V-bdc-

L2 (L2 = tpt, tppy, tpbz), V-abdc-L2 (L2 = tpt, tppy, tpbz), V-Brbdc-L2 (L2 = tppy, tpbz), V-bcp-L2 (L2 = tpt, tppy, tpbz), V-L1-tph (L1 = chdc, 26ndc, bpdc) (Scheme 1).

For isoreticular chemistry, if the variation in each module is denoted as n1, n2, n3 etc., the maximum number of isoreticular phases would be the product of these numbers. The percentage of those theoretically possible phases that have actually been synthesized is defined here as Isoreticular Realization Factor (IRF). In this work, a value of 50% IRF (14 synthesized phases out of 28 possibilities) is realized for the L1-L2 combinations. The IRF values can be increased by additional synthetic efforts. However, clearly, there is a maximum achievable value. Different platforms will have different synthetically achievable maximum IRF values reflecting the tolerance of each platform towards isoreticular replacement. This work has shown a rich isoreticular chemistry in V-MOF system and opens up many opportunities to tune both pore size and shape with either L1 or L2 ligand as well as with both of them.

A range of structural and gas sorption properties have been achieved. The *c*/*a* ratio of the hexagonal unit cell which is a quantifying number for the pore shape ranges from 0.612 for V-chdc-tph (also called CPM-220h-V) to 1.258 for V-bpdc-tph (also called CPM-737h), indicative of the remarkable control over pore geometry. As a result, the porosity, gas uptake and separation properties for many gases such as CO_2/C_2H_2, C_2H_4/C_2H_6, and C_3H_6/C_3H_8 can be varied to a great extent. The BET surface area can be tuned from 820 for V-bcp-tpbz to 2964 $m^2\ g^{-1}$ for V-bpdc-tph. With exceptional uptake for C_2H_2 (182 $cm^3\ g^{-1}$ at 298 K and 1 bar for V-bdc-tpt) and a tunable C_2H_2/CO_2 selectivity (e.g., 3.3 for V-bdc-tpt, 11.0 for V-bcp-tppy at 298 K), these materials are promising for C_2H_2/CO_2 separation as confirmed by the experimental breakthrough data for V-bdc-tpt.

The new V-*pacs* also have extraordinary capacity for C_2H_6 (166.8 $cm^3\ g^{-1}$ at 298 K and 1 bar for V-bdc-tpt) and highly desirable C_2H_6-selective C_2H_6/C_2H_4 selectivity (1.43 at 298 K for V-bdc-tpt). The ability of V-bdc-tpt to separate C_2H_6/C_2H_4 has been confirmed by the breakthrough experiments. New V-MOFs also have high uptake capacity for C_3H_6 (229.1 for V-bdc-tpt and 270.8 $cm^3\ g^{-1}$ for V-bpdc-tph) and C_3H_8 (209.9 for V-bdc-tpt and 254.9 $cm^3\ g^{-1}$ for V-bpdc-tph) at 298 K and 1 bar. Remarkably, V-bdc-tpt is believed to have the highest uptake capacity at 0.1 bar and 298 K for both C_3H_6 (167.7 $cm^3\ g^{-1}$) and C_3H_8 (161.1 $cm^3\ g^{-1}$), whereas the C_3H_8 uptake capacity (254.9 $cm^3\ g^{-1}$ for V-bpdc-tph) at 298 K and 1 bar is likely the highest among C_3H_8-selective materials. Through dual-ligand isoreticular chemistry taking advantage of both L1 and L2 tunability, we can tune the pore size and geometry in both small and large increments either anisotropically along crystallographic *a*/*b* or *c* directions or nearly isotropically by scaling *a*/*b* and *c* axes in similar proportions. In one example, the isoreticular

modification from V-bdc-tpt to V-bpdc-tph profoundly changed the selectivity from C_3H_6-selective by V-bdc-tpt to C_3H_8-selective by V-bpdc-tph. The high C_3H_8 uptake (11.37 mmol g^{-1}) by V-bpdc-tph contributes to its high separation potential (1.24 mmol g^{-1}) for C_3H_8/C_3H_6 (50:50 v/v) mixture. With V-bpdc-tph, we have also demonstrated that its separation potential can be enhanced by a small change in temperature (from 0.79 at 298 K to 2.11 at 273 K for C_2H_6-selective C_2H_4/C_2H_6 separation). For C_3H_8-selective separation of C_3H_6/C_3H_8, the separation potential peaks at 313K at 1.38, as compared to 1.25 at 298 K.

2. Result and discussion

2.1. Isoreticular design and pore space partition of an extensible family of V-MOF.

A major advance of this work is the large number of new porous V-MOFs that have now been accessible or will be accessible using the approach reported here. Here, after sampling just a fraction of the L1-L2 combinations, a series of 14 V-*pacs* materials were successfully synthesized by co-assembly between V-trimer, various dicarboxylate ligands and tripyridyl ligands. As confirmed by powder X-ray diffraction (Figures S1), all could be made in the pure form except for two phases (V-bcp-tpt and V-26ndc-tph) for which further optimization of synthesis conditions is still needed. They crystallized in hexagonal $P6_3/mmc$ space group or its subgroup P-31c (for V-26ndc-tph only) (Tables S1-S3). A typical reaction for crystal growth involves a mixture of VCl_3, L1 ligand, L2 ligand in N,N-dimethylformamide (DMF) at 150 °C for 12 hrs. A small amount of 6 M HCl may be used to help increase the size of crystals, but is not essential for producing pure phases of these V-MOFs. The crystal size of V-bdc-tpbz, V-abdc-tpt and V-bpdc-tph is around 100 μm (Figure 1a), sufficiently large for obtaining high-quality single-crystal X-ray diffraction data for accurate structure analysis.

To demonstrate the broad scope of the isoreticular chemistry in V-MOFs as well as to enable the control over gas sorption properties, we used 7 chemically representative L1 ligands and 4 different L2 ligands with either subtle structural change or large change (Table S2). For L1 ligands, in addition to the prototypical aromatic bdc ligand, we selected two ligands from each of the three categories. The first category is based on the ligand substitution or functionalization and here we selected two mono-substituted versions with both small (-NH_2) and large (-Br) substituents. The steric effect from large substituents such as -Br could have great impact on the resonance structure of L1 and the associated coplanarity between -COO groups and phenyl rings, which is an interesting factor to consider in the *pacs* crystallization process. The second category is based on the geometric scaling of bdc while maintaining colinear orientation of two -COO groups. Here we selected the elongated versions of bdc: 2,6-ndc with fused aromatic

Table 1. Summary of some crystallographic parameters of all V-*pacs* in this work.

Sample code	Space group	*a* axis (Å)	*c* axis (Å)	Cell volume (Å^3)	*c*/*a* ratio	*R* factor
V-bdc-tpt	*P*6$_3$/*mmc*	16.7765(18)	14.510(2)	3536.8(10)	0.865	0.053
V-bdc-tppy	*P*6$_3$/*mmc*	16.9142(7)	14.3789(10)	3562.5(4)	0.850	0.077
V-bdc-tpbz	*P*6$_3$/*mmc*	16.9601(6)	14.6377(7)	3646.4(3)	0.863	0.039
V-abdc-tpt	*P*6$_3$/*mmc*	16.7009(13)	15.039(2)	3632.8(8)	0.900	0.059
V-abdc-tppy	*P*6$_3$/*mmc*	16.906(2)	14.525(3)	3595.3(11)	0.859	0.068
V-abdc-tpbz	*P*6$_3$/*mmc*	16.9998(16)	14.454(3)	3617.4(10)	0.850	0.072
V-Brbdc-tppy[a)]	*P*6$_3$/*mmc*	16.818	14.636	3584.8	0.870	-
V-Brbdc-tpbz[a)]	*P*6$_3$/*mmc*	16.919	14.511	3597.3	0.858	-
V-bcp-tpt	*P*6$_3$/*mmc*	16.6976(11)	11.8917(13)	2871.3(5)	0.712	0.090
V-bcp-tppy	*P*6$_3$/*mmc*	16.866(3)	11.230(4)	2766.6(14)	0.666	0.14
V-bcp-tpbz	*P*6$_3$/*mmc*	16.997(3)	11.130(4)	2784.9(14)	0.655	0.19
V-26ndc-tph	*P*-31*c*	18.964(7)	18.408(12)	5733(6)	0.971	0.10
V-bpdc-tph	*P*6$_3$/*mmc*	19.0197(18)	23.932(4)	7497.4(18)	1.258	0.060
V-chdc-tph[a)]	*P*6$_3$/*mmc*	18.810	11.510	3526.7	0.612	-

a) Unit cell is calculated by powder X-ray diffraction data.

rings and offset bonding vectors (by about one C-C bond distance) and bpdc with non-fused biphenyl-based ligand and no offset in two bonding vectors. It is worth noting that due to the high symmetry of the *pacs* topological net (2/*m* symmetry at the L1 site with m symmetry bisecting two -COO groups and 2-fold axis perpendicular to the bonding vectors between -COO and trimers), the offset in the carboxylate bonding vectors could have significant impact in the crystallization process due to the order-disorder phenomenon. The third category of ligands follows a new trend in the MOF design which is the use of the concept called bioisosteric (BIS) replacement method. This BIS method is a strategy to use non-aromatic ligands to mimic the benzene-based molecules. Here we selected one monocyclic and flexible ligand (chdc) and one bicyclic rigid ligand (bcp) to demonstrate the broad applicability of our synthesis approach.

For L2 ligands, in addition to the prototypical tpt ligand with triazine core (C/N ratio 3/3), tppy with pyridine core (C/N ratio 5/1) and tpbz with benzene core (C/N ratio 6/0) are used. The minor difference between the bond lengths of C-N and C-C can lead to small changes in the pore size which translates into different gas selectivity. The cores in tpt, tppy, and tpbz are collectively called X6 core. In addition, tph ligand with an expanded core size (X13) was used in this work which enables an extra level of control over porosity.

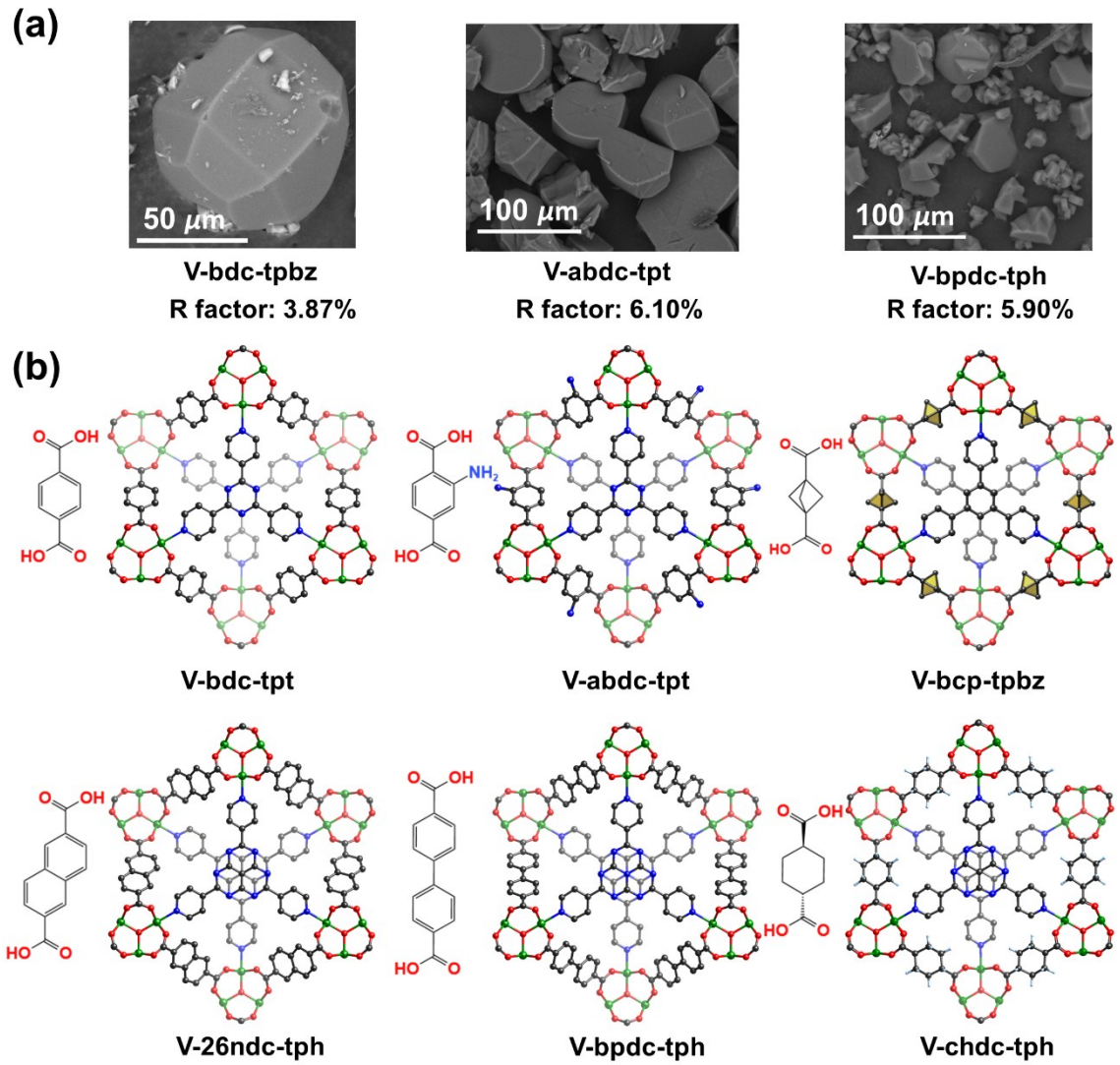

Figure 1. (a) Large single crystals of new V-bdc-tpbz, V-abdc-tpt and V-bpdc-tph. (b) Six new V-MOFs with different L1-L2 combinations showing pore size/shape tuning by L1/L2 and pore-space partition by L2 ligands.

In the discussion of these new V-MOFs, first we would like to highlight the improvement in the stability and porosity of V-MOFs in this work as compared to previously reported V-MOFs. The most informative comparison is between V-bdc-tpt in this work and previously reported V-MIL-88B,[18] because these two materials share the common trimers and L1 ligands. V-bdc-tpt-*pacs* has far superior properties than V-MIL-88B. This is because V-bdc-tpt has an extra pore-partition ligand (L2), making V-bdc-tpt rigid whereas V-MIL-88B is soft. We can use *c*/*a* ratio and cell volume to quantify the difference between V-bdc-tpt-*pacs* and V-MIL-88B. Since the porous channel runs along the hexagonal *c* axis, the lengths of the *a*/*b* axes are a measure of the diameter of channels. As the *c*/*a* ratio increases, the framework channel of MIL-88B can

be perceived as narrowing down towards less open phases and eventually ending up with the closed non-porous phase. The *c*/*a* ratios of closed and open V-MIL-88B are 1.79 and 1.01. In comparison, the *c*/*a* ratio of V-bdc-tpt-*pacs* is 0.865, even smaller than the open phase (methanol) of V-MIL-88B. In other words, it can be said that the pore-space-partitioned V-bdc-tpt is more open than the most open MIL-88 phase. Similarly, the cell volume of V-bdc-tpt is 3537 $Å^3$, larger than 1923 $Å^3$ for the closed phase and 3419 $Å^3$ for the open phase (methanol) of V-MIL-88B.

The pore geometry and adsorption properties of V-bdc-tpt can be fine-tuned by replacing L2 ligand (tpt) with tppy or tpbz, which leads to a subtle change in the *c*/*a* ratio from 0.865 to 0.850 for V-bdc-tppy and 0.863 for V-bdc-tpbz and a small change in the unit-cell volume from 3537 $Å^3$ to 3562 $Å^3$ and 3646 $Å^3$ (Table S3). Such porosity control at a very fine level comes from the minor size differences in these X6-type L2 ligands and makes it possible to tune separation selectivity for gas mixtures, especially when the pore size is very close to the size of the guest molecules.

In addition to the variation in L2 ligands (from tpt to tppy and tpbz) starting from V-bdc-tpt, amino- and bromo-substituted bdc ligands were also studied as L1 ligand, which led to the synthesis of five V-*pacs* materials, V-abdc-tpt, V-abdc-tppy, V-abdc-tpbz, V-Brbdc-tppy, and V-Brbdc-tpbz. Given the rich substitution chemistry of dicarboxylic acid ligands, we can expect that a large number of V-MOFs can be synthesized with this strategy. It is worth noting that while tpt, tppy, and tpbz play similar structural roles, their behaviors during the synthesis can be quite different as evidenced by the fact that V-Brbdc-tpt is not yet synthesized.

To realize greater variations in pore size and shape, additional strategies such as bioisosteric replacement were used. For the same L2 ligand, the *c*/*a* ratio can be tuned with different L1 ligands. When aromatic bdc is replaced with bioisosteric sp^3-carbon-based bcp ligand, three V-bcp *pacs* materials that directly correspond to three V-bdc *pacs* materials were synthesized. The smaller bcp ligand (compared with bdc) gives rise to a significant decrease in the *c*/*a* ratio: 0.865 to 0.712 from V-bdc-tpt to V-bcp-tpt, 0.850 to 0.666 from V-bdc-tppy to V-bcp-tppy, and 0.863 to 0.655 from V-bdc-tpbz to V-bcp-tpbz (Table S3). The most notable effect of using short bcp ligand is a significant increase in the C_2H_2/CO_2 selectivity from about 3.3 for V-bdc-tpt to 11.0 for V-bcp-tppy and 10.1 for V-bcp-tpbz (sorption data for V-bcp-tpt not measured due to the presence of impurity).

Unique to V-MOFs are three new V-*pacs* materials (i.e., V-chdc-tph, V-26ndc-tph, V-bpdc-tph) made from pore-partition L2 ligand tph. Such L1-L2 combinations are novel and not yet known in MOFs made from other high-valent metals such as Al, In, or Cr. One unique feature

is that tph ligand is anionic which is uncommon among pore-partition L2 ligands. In traditional *pacs* materials with neutral frameworks, L2 ligands (e.g., tpt, tppy, tpbz) are neutral, so that the framework neutralization occurs at the interface between the trimer and COO- groups. This can be regarded as a form of local-charge balance between each trimer and six surrounding L1 ligands. In comparison, the charge neutralization in the V-L1-tph-pacs also involves trimer clusters and L2 ligands. Since the charge of tph is centered at its core, it is far away from the trimer. This can be considered as a form of the global-charge balance similar to that between the host framework and guest counter anions.

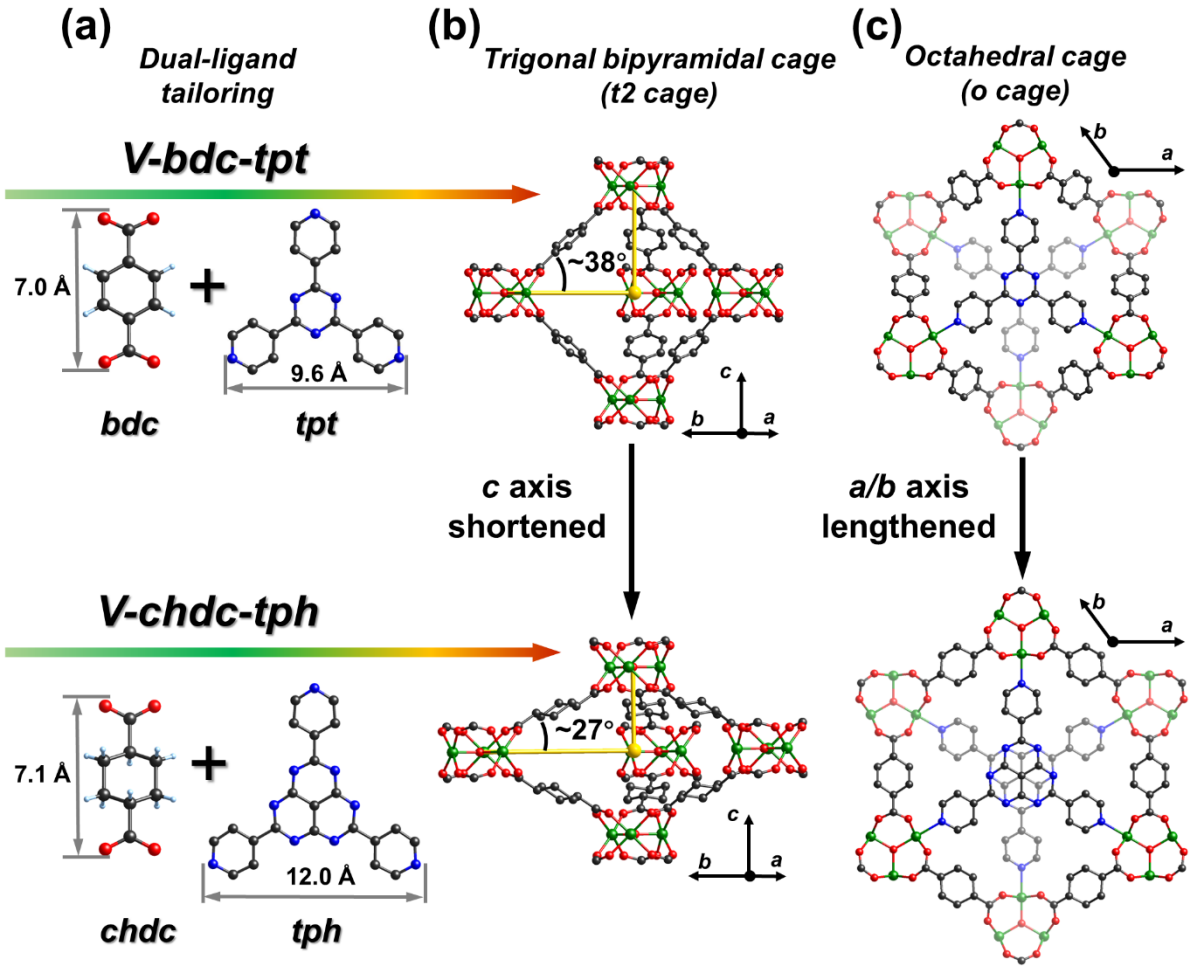

Figure 2. Multi-modular isoreticular tailoring of pore space in V-bdc-tpt (CPM-717a) and V-chdc-tph (CPM-220h). (a) L1 and L2 ligands as two different modules with different structural roles (framework-forming by L1 and pore partition by L2). (b) trigonal bipyramidal cage (t_2 cage) is compressed from 38° in V-bdc-tpt to 27° in V-chdc-tph, mostly due to the core expansion from tpt to tph. (c) the partition of hexagonal channel by tpt (top) and tph (bottom) into octahedral cage (o cage) in V-bdc-tpt and V-chdc-tph, respectively.

One V-MOF that pushes the synthetic and structural limits of the *pacs* platform is V-chdc-tph because of the unprecedented combination between small L1 ligand chdc and large L2 ligand tph (Figure 2). In general, the *pacs* platform can tolerate a significant size difference between L1 and L2 ligands. However, there is a lack of study correlating the range of L1/L2 length ratios with synthetically accessible pacs structures. Some seemingly impossible combinations have been encountered sporadically. Prior to this work, three smallest ditopic ligands that can combine with tph are H_2tba (4-(1*H*-tetrazol-5-yl)benzoic acid, 8.4 Å), Hcpt (4-(*p*-carboxyphenyl)-1,2,4-triazole, 8.4 Å), and 26ndc (9.1 Å). Many synthetic efforts to integrate bdc (6.9 Å) and tph in *pacs* have so far yielded no results in all metal compositions. Thus the success in combining chdc (which has a size only slightly larger than bdc, 7.1 Å vs. 6.9 Å) and tph is extraordinary. The large size difference (around 5 Å) between L1 and L2 (7.1 Å vs. 12.0 Å) gives rise to a very high level of compression of trigonal bipyramidal cage and octahedral cage in V-chdc-tph. A small *c*/*a* ratio and the associated compression of cages are known for contributing to high selectivity in gas separation. In the design of new *pacs* materials, there have been a continual effort to decrease the *c*/*a* ratio. Usually, these studies have centered on the use of small L1 ligand such as bcp and tcb (tcb = *trans*-1,3-cyclobutanedicarboxylic acid) with standard X6 L2 ligands (e.g., tpt, tppy, tpbz) which have led to a *c*/*a* ratio as low as 0.574 in CoV-tcb-tpbz-act by shortening the *c* axis while keeping the *a* axis nearly constant.[46] However, the limitation of this method includes the difficulty in combining these L1 ligands (e.g., bcp and tcb) with larger L2 ligand such as tph. In fact, even bdc ligand which is larger than bcp and tcb ligands have not been found to co-assemble with tph. In this work, we demonstrate an alternative and yet highly effective method through the combination between a conformationally flexible chdc ligand and tph. This allows us to reach a low *c*/*a* ratio of 0.612 in V-chdc-tph. This value is the lowest among all V-MOFs reported here. With further refinement on this chdc-tph strategy, it is promising to push the *c*/*a* ratio even lower.

2.2. Gas sorption and separation properties of new vanadium MOFs.

2.2.1 Pore characterization of V-*pacs*

V-*pacs* are desolvated by guest exchange with acetone first followed by activation under high vacuum at 50 °C. The porosity of V-*pacs* is characterized by N_2 isotherm at 77 K. The Brunauer–Emmett–Teller (BET) surface area of V-bdc-tpt (also called CPM-717a) is 1720 m^2 g^{-1} (Figure 3a), which is higher than V-bdc-tppy (1670 m^2 g^{-1}) and V-bdc-tpbz (1460 m^2 g^{-1}) (Figure S3). In fact, V-bdc-tpt has the highest BET surface area among all bdc-based *pacs* including CoV-bdc-tpt[32] (1328 m^2 g^{-1}), MgV-bdc-tpt[31] (1320 m^2 g^{-1}), Ni-bdc-tpt[26] (966 m^2

g^{-1}) and Cr-bdc-tpt[38] (1123 m^2 g^{-1}). The pore size distribution of V-bdc-tpt peaks at 5.0 Å and 6.4 Å (Figure S3), likely corresponding to the size set by the octahedral cage and trigonal bipyramidal cage, respectively. By tuning the size of L1 or L2 ligands, the pore size of these V-MOFs can be increased from 6.4 Å to 10.9 Å. V-bpdc-tph has the highest BET surface area of 2964 m^2 g^{-1} among all *pacs* materials. It is higher than heterometallic CoV-bpdc-tph (2260 m^2 g^{-1})[39] with the same L1 and L2 ligands. The pore volume of 1.18 cm^3 g^{-1} is also the highest one in all *pacs*.

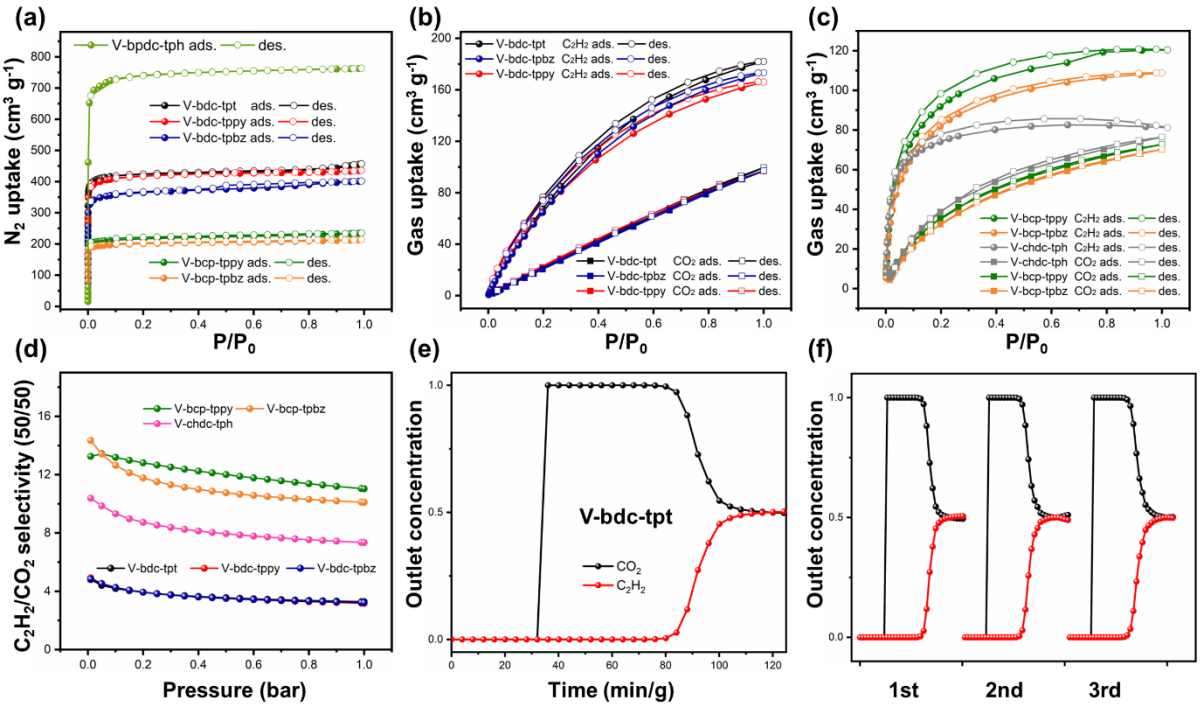

Figure 3. N_2, C_2H_2 and CO_2 sorption and breakthrough experiments of V-*pacs*. (a) N_2 sorption isotherms of V-*pacs* at 77 K. C_2H_2 and CO_2 sorption isotherms at 1 bar and 298 K for V-bdc-X6 (b), V-bcp-X6 and V-chdc-tph (c). (d) C_2H_2/CO_2 selectivity (50:50) at 1 bar and 298 K. (e) C_2H_2 and CO_2 breakthrough curve and (f) 3 cycles of measurements.

2.2.2 C_2H_2/CO_2 uptake and separation

V-bdc-tpt shows high CO_2 and C_2H_2 uptakes. The CO_2 uptake of V-bdc-tpt is 99.5 cm^3 g^{-1} and 189.2 cm^3 g^{-1} at 1 bar, 298 K and 273 K (Figure 3b), respectively, which is higher than CPM-733-CoV[32] (83.6 cm^3 g^{-1} and 170.8 cm^3 g^{-1}) and CPM-233-MgV[32] (90.5 cm^3 g^{-1} and 171.4 cm^3 g^{-1}) at 298 K and 273 K, respectively. The C_2H_2 uptake of V-bdc-tpt is 182.0 cm^3 g^{-1} and 262.0 cm^3 g^{-1} at 298 K and 273 K, respectively, which is higher than CPM-733 (162.0 cm^3 g^{-1} and 249.4 cm^3 g^{-1}), but slightly lower than CPM-233 (193.7 cm^3 g^{-1} and 266.8 cm^3 g^{-1}) at 298 K and 273 K, respectively (Table S13). V-bcp-tppy, V-bcp-tpbz and V-chdc-tph show

high C_2H_2 uptake at 0.1 bar and 298K (78.1 $cm^3\ g^{-1}$, 68.8 $cm^3\ g^{-1}$, 68.1 $cm^3\ g^{-1}$, respectively) leading to a high ratio (65.0%, 63.2%, 84.0%, respectively) for uptakes at 0.1 bar over 1 bar (Figure 3c, Table S14), indicative of the strong affinity for C_2H_2 molecules.

The C_2H_2/CO_2 selectivity of V-bdc-tpt is 3.3, higher than CPM-733 (2.6) and CPM-233 (2.7), which indicates the better C_2H_2/CO_2 separation ability than heterometallic bdc-*pacs*. The selectivity of V-bcp-tppy, V-bcp-tpbz and V-chdc-tph are 11.0, 10.1 and 7.3 (Figure 3d), which is higher than ZJNU-13[50] (5.6) and ZJNU-118[51] (4.5). V-bcp-tppy shows the highest selectivity (11.0) and separation potential (4.2 mmol g^{-1}) in V-*pacs*.

The fixed-bed breakthrough measurement was performed with 2 mL min^{-1} mixed gas flow rate (C_2H_2/CO_2 = 1/1, v/v) at 298 K using V-bdc-tpt (experimental detail in supporting information). As shown in Figure 3e, C_2H_2/CO_2 mixture could be separated by V-bdc-tpt. CO_2 quickly broke through from the column, whereas C_2H_2 was retained in the column for additional ~48 min g^{-1}, which demonstrates the separation ability of V-bdc-tpt. The C_2H_2/CO_2 breakthrough time is longer than many benchmark MOF materials with the same gas flow rate (2 mL min^{-1}), such as UTSA-300a[52] (12 min g^{-1}), ZJU-74a[53] (36 min g^{-1}), FJU-90a[48] (22 min g^{-1}) and SNNU-27-Fe[49] (45 min g^{-1}). Multicycle mixed-gas breakthrough experiments are carried out under the same conditions. Breakthrough time is the same for three runs of experiment (Figure 3f), confirming the stability of V-bdc-tpt.

2.2.3 C_2H_6-selective C_2H_6/C_2H_4 separation

V-bdc-tpt shows very high C_2H_6 uptake at 1 bar, 298 K and 273 K. The C_2H_6 uptake of V-bdc-tpt is 166.8 $cm^3\ g^{-1}$ at 1 bar and 298 K (Figure 4a), which is the same as high C_2H_6 uptake MOF material CPM-223 (166.8 $cm^3\ g^{-1}$), and slightly lower than the highest C_2H_6 uptake MOF material SNNU-40[54] (169.0 $cm^3\ g^{-1}$) (Figure 4b, Table S15). It is notable that even though the surface areas of *pacs* materials are not high compared to most porous MOFs, their C_2H_6 uptakes are at or near record high. V-bdc-tpt shows higher C_2H_6 uptake than ZJU-60[55] and Mg-MOF-74[56] with the similar surface areas about 1700 $m^2\ g^{-1}$ (Figure 4c).

The C_2H_6 uptake of V-bdc-tpt is 208.5 $cm^3\ g^{-1}$ at 1 bar and 273 K (Figures S5). This uptake value is comparable to the reported MOFs with top C_2H_6 uptake capacity at 273 K, such as UMCM-150[57] (208 $cm^3\ g^{-1}$), Cu-TDPAT[58] (218 $cm^3\ g^{-1}$) and ZJU-11[59] (230 $cm^3\ g^{-1}$). The uptake capacity of V-bdc-tpt is also higher than all heterometallic *pacs* such as CPM-733[32] (Co_2V trimer, 186.3 $cm^3\ g^{-1}$), CPM-223[32] (Mg_2Ti trimer, 190.8 $cm^3\ g^{-1}$), and CPM-233[32] (Mg_2V trimer, 178.6 $cm^3\ g^{-1}$) (Table S8).

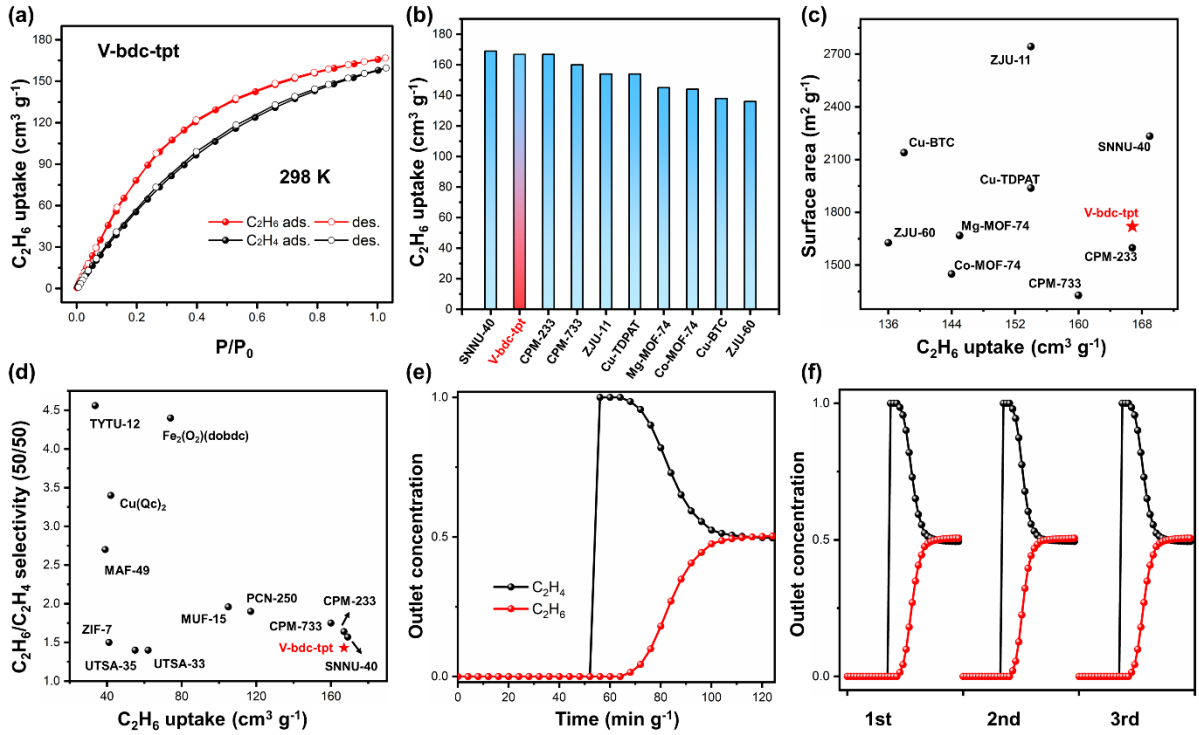

Figure 4. C_2H_6, C_2H_4 sorption and breakthrough experiments of V-bdc-tpt. (a) C_2H_6 and C_2H_4 isotherms 298 K. (b) Comparison of C_2H_6 uptakes at 298K and 1 bar with other high-capacity MOFs. (c) Comparison of C_2H_6 uptake capacity *vs*. surface area for various high-performance MOFs, showing very high C_2H_6 uptake by V-bdc-tpt despite its modest surface area. (d) comparison of C_2H_6 uptake capacity *vs*. C_2H_6/C_2H_4 selectivity (50:50) for high-performance MOF materials. (e) breakthrough curve for C_2H_6-selective C_2H_6/C_2H_4 separation and (f) 3 cycles of breakthrough measurements.

V-bdc-tpt shows highly desirable C_2H_6 selectivity over C_2H_4. The C_2H_6-C_2H_4 selectivity (50/50, v/v) of V-bdc-tpt is 1.43 at 1 bar and 298 K (Figure 4d). It is higher than UTSA-33[60] (1.4) and UTSA-35[61] (1.4), but lower than ZNJU-21[62] (1.7), CPM-733[32] (1.75) and TYTU-12[63] (4.6). The separation potential is 1.29 mmol g^{-1}, which surpasses some benchmark MOF materials such as $Ni(BDC)(TED)_{0.5}$[64] (1.01 mmol g^{-1}), $Cu(Qc)_2$[65] (0.85 mmol g^{-1}), MAF-49[66] (0.78 mmol g^{-1}) and ZIF-8[67] (0.56 mmol g^{-1}) (Table S15). The fixed-bed breakthrough measurement was performed with 2 mL min^{-1} total gas flow rate (C_2H_6/C_2H_4 = 1/1, v/v) at 298 K for V-bdc-tpt. As shown in Figure 4e, C_2H_6/C_2H_4 mixture could be completely separated by V-bdc-tpt. C_2H_4 quickly broke through from the column, whereas C_2H_6 was retained in the column for additional ~15 min g^{-1}. Multicycle mixed-gas breakthrough experiments show the same breakthrough time for three runs, suggesting the high stability of V-bdc-tpt (Figure 4f).

V-bpdc-tph also shows C_2H_6 selectivity over C_2H_4 (Figure S5.6-S5.8). Its C_2H_6-C_2H_4 selectivity (50/50, v/v) is 1.49 at 298 K and increases to 1.63 at 273 K. The separation potential is 0.79 mmol g^{-1} at 298 K, which is lower than V-bdc-tpt. At 273 K, it has very high separation potential of 2.1 mmol g^{-1} (Table S9).

2.2.4 C_3H_8 and C_3H_6 uptake and storage

V-bdc-tpt (CPM-717a) and V-bpdc-tph (CPM-737h) with different pore properties were selected to study adsorption properties of propane and propene. The C_3H_8 uptake of V-bdc-tpt is 209.9 cm^3 g^{-1} at 1 atm and 298 K (Figure 5a), which is higher than BUT-10[68] (134.0 cm^3 g^{-1}), MIL-100(Fe)[69] (151.8 cm^3 g^{-1}), Zr-bipy[68] (180.0 cm^3 g^{-1}). The C_3H_6 uptake of V-bdc-tpt is 229.1 cm^3 g^{-1} at 1 bar and 298 K, which is higher than UiO-67[68] (220.0 cm^3 g^{-1}). Note that the C3 light hydrocarbon uptake of V-bdc-tpt is also higher than some *pacs* materials with similar pore size (6~7 Å), such as CoV-bcp-tpt[41] (84.9 cm^3 g^{-1} for C_3H_8, 92.1 cm^3 g^{-1} for C_3H_6), CoV-bco-tpt[45] (110.4 cm^3 g^{-1} for C_3H_8, 110.0 cm^3 g^{-1} for C_3H_6) and CoV-bdc-tpt[41] (170.2 cm^3 g^{-1} for C_3H_8, 168.7 cm^3 g^{-1} for C_3H_6). The C3 uptake at 298 K and 1bar of V-bdc-tpt (209.9 and 229.1 cm^3 g^{-1} for C_3H_8 and C_3H_6) is also higher than larger-pore-sized *pacs* materials such as CoV-26ndc-tph[39] (176.0 and 188.4 cm^3 g^{-1}) and CoV-bdt-tph[39] (208.0 and 226.2 cm^3 g^{-1}) (Table S9).

In addition to high C3 uptakes at 1 bar, V-bdc-tpt also has very high C_3H_8 (161.1 cm^3 g^{-1}) and C_3H_6 (167.1 cm^3 g^{-1}) uptake at 0.1 bar and 298 K (Figures 5b, c), which surpasses many benchmark MOF materials such as BUT-10[68] (105.0 and 79.0 cm^3 g^{-1} for C_3H_8 and C_3H_6), Iso-MOF-4[70] (101.5 and 74.0 cm^3 g^{-1}), FJI-H23[71] (100.0 and 133.0 cm^3 g^{-1}), Zr-bipy[68] (60.5 and 44.0 cm^3 g^{-1}), UiO-67[68] (55.0 and 63.0 cm^3 g^{-1}), and MIL-100(Fe)[69] (33.6 cm^3 g^{-1} for C_3H_8). This is believed to be the highest C_3H_8 and C_3H_6 uptake at 0.1 bar and 298 K (Figures 5d, Table S16).

V-bdc-tpt and V-bpdc-tph show different behaviors for the adsorption of C3 gases. V-bdc-tpt is a small-pore (6.4 Å) material with strong affinity for gas molecules as shown by very high uptake at low pressure. The isosteric heat of C_3H_8 and C_3H_6 is 35.7 kJ mol^{-1} and 33.5 kJ mol^{-1}, respectively. In comparison, V-bpdc-tph is a large-pore (10.9 Å) materials with high BET surface area and pore volume. The low-pressure (0.1 bar) uptake of V-bpdc-tph is relatively low, however, it has a very high total uptake (254.9 cm^3 g^{-1} at 298 K and 1 bar). The isosteric heat of C_3H_8 and C_3H_6 is 20.9 kJ mol^{-1} and 20.5 kJ mol^{-1}, respectively, much smaller than V-bdc-tpt. The C3 isotherms of V-bpdc-tph shows different shape form V-bdc-tpt (Figure S6.4).

For V-bdc-tpt, it is Type-I-like curve with a rapid uptake at low pressure (around 0.1 bar). For V-bpdc-tph, at the low-pressure area, the increase in the uptake is more gradual.

The pore expansion from V-bdc-tpt to V-bpdc-tph shows considerable effect on the uptake of C_3H_8 and C_3H_6. V-bpdc-tph adsorbs 254.9 $cm^3\ g^{-1}$ C_3H_8 and 270.8 $cm^3\ g^{-1}$ C_3H_6 at 1 bar and 298 K (Figure 5e). The C_3H_8 and C_3H_6 uptake is slightly lower than FJI-H23[71], but is higher than all other *pacs* materials including other V-MOFs reported here (Figures 5b, c). Interestingly, V-bpdc-tph is a C_3H_8 selective material for C_3H_8/C_3H_6 (50/50, v/v) at 1 bar and 298 K. The selectivity of V-bpdc-tph is 1.24 at 1 bar and 298 K (Figure 5f), which is higher than UiO-67[68] (1.07), but lower than CPM-734c[37] (1.44) and FDMOF-2[72] (2.18). The separation potential is 1.25 mmol g^{-1}, which surpasses some benchmark MOF materials such as CPM-736t[37] (1.24 mmol g^{-1}), BUT-10[68] (1.04 mmol g^{-1}), Zr-bipy[68] (0.91 mmol g^{-1}), UiO-67[68] (0.43 mmol g^{-1}) and ZIF-8[67] (0.12 mmol g^{-1}) (Table S17), but is lower than FDMOF-2[72] (1.78 mmol g^{-1}).

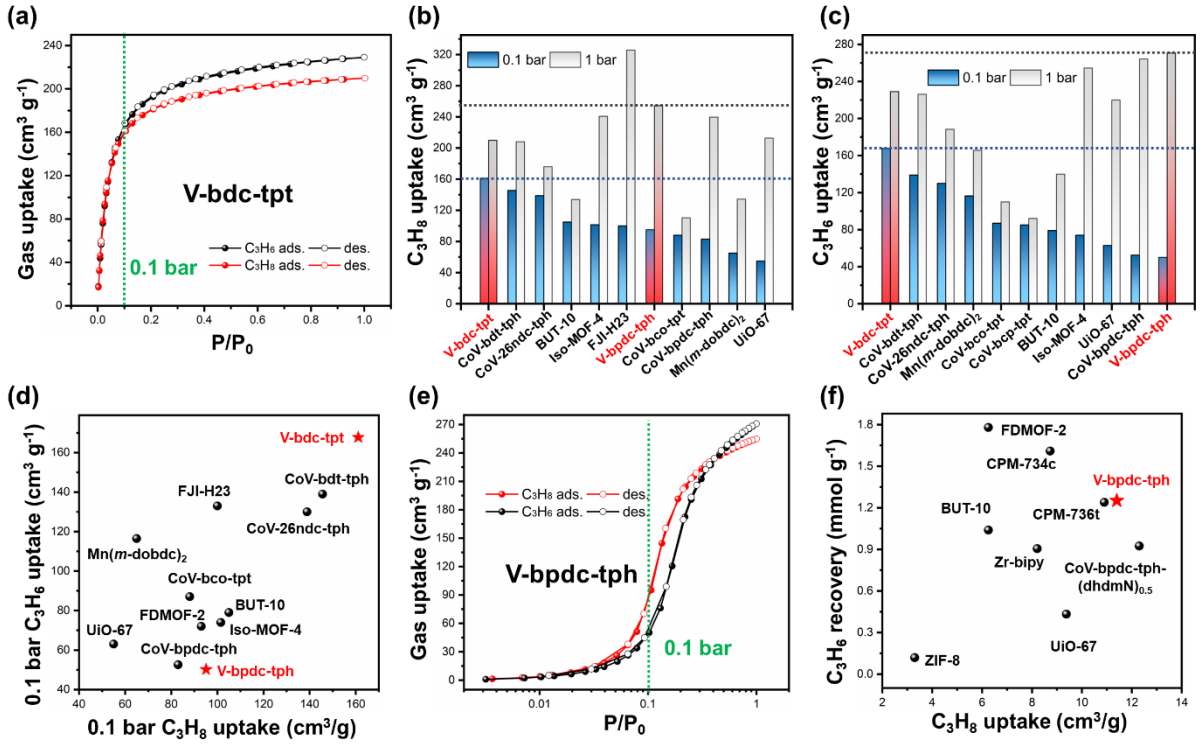

Figure 5. (a) C_3H_8 and C_3H_6 sorption isotherms of V-bdc-tpt at 298 K. Comparison of 0.1 and 1 bar C_3H_8 uptake (b) and C_3H_6 uptake (c) of V-bdc-tpt and V-bpdc-tph with other high-capacity MOFs at 298 K. (d) 0.1 bar C_3H_8 and C_3H_6 uptake comparison of V-bdc-tpt with other MOFs at 298 K. (e) C_3H_8 and C_3H_6 sorption isotherms of V-bpdc-tph at 298 K. (f) Comparison of C_3H_6/C_3H_8 separation properties of V-bpdc-tph with other C_3H_8-selective MOF materials.

3. Conclusion

With the successful synthesis of a family of new porous V-MOFs, this work demonstrates the great promise of vanadium for the construction of crystalline porous materials. As shown here, V-MOFs have properties that are superior to structurally comparable MOFs made from other metal ions. Unfortunately, the synthesis of V-MOFs has not received adequate attention for some time, likely due to the perceived difficulty of solvothermal vanadium MOF chemistry that is riddled with competing crystallization pathways. Hopefully, this work will inspire a renewed enthusiasm on the fundamental chemistry of V-MOF synthesis and their applications. Like its two neighbors (Ti and Cr), vanadium is one of the most unique elements in the periodic table and porous materials based on vanadium have a great potential for generating new applications.

Supporting Information

Supporting Information is available from the Wiley Online Library or from the author. Detail experimental procedures, materials characterization, single crystallographic parameters, and gas sorption data are included in supporting information.

Acknowledgements

This work was supported by National Science Foundation, Division of Materials Research, under Award # 2105961 (X. B.). Single-crystal X-ray diffraction studies were performed on an instrument purchased with an NSF MRI grant (CHEM 2117040, X.B.). X.B. thanks the RSCA award for teaching release time from CSULB.

Received: ((will be filled in by the editorial staff))
Revised: ((will be filled in by the editorial staff))
Published online: ((will be filled in by the editorial staff))

Reference

[1] H. Yang, T. X. Trieu, X. Zhao, Y. Wang, Y. Wang, P. Feng, X. Bu, *Angew. Chem. Int. Ed.* **2019**, *58*, 11757-11762.

[2] A. F. Cozzolino, C. K. Brozek, R. D. Palmer, J. Yano, M. Li, M. Dincă, *J. Am. Chem. Soc.* **2014**, *136*, 3334-3337.

[3] H. Li, M. Eddaoudi, M. O'Keeffe, O. M. Yaghi, *Nature* **1999**, *402*, 276-279.

[4] G. Ferey, C. Serre, *Chem. Soc. Rev.* **2009**, *38*, 1380-1399.

[5] L. Feng, G. S. Day, K.-Y. Wang, S. Yuan, H.-C. Zhou, *Chem* **2020**, *6*, 2902-2923.

[6] W. Fan, K.-Y. Wang, C. Welton, L. Feng, X. Wang, X. Liu, Y. Li, Z. Kang, H.-C. Zhou, R. Wang, D. Sun, *Coord. Chem. Rev.* **2023**, *489*, 215175.

[7] P. Van Der Voort, K. Leus, Y.-Y. Liu, M. Vandichel, V. Van Speybroeck, M. Waroquier, S. Biswas, *New J. Chem.* **2014**, *38*, 1853-1867.

[8] C. Wang, J. Yan, S. Chen, Y. Liu, *ChemPlusChem* **2023**, *88*, e202200462.

[9] X. Zhao, C. Mao, K. T. Luong, Q. Lin, Q.-G. Zhai, P. Feng, X. Bu, *Angew. Chem. Int. Ed.* **2016**, *55*, 2768-2772.

[10] H. Yang, F. Peng, A. N. Hong, Y. Wang, X. Bu, P. Feng, *J. Am. Chem. Soc.* **2021**, *143*, 14470-14474.

[11] K. Barthelet, J. Marrot, D. Riou, G. Férey, *Angew. Chem. Int. Ed.* **2002**, *41*, 281-284.

[12] K. Barthelet, J. Marrot, G. Férey, D. Riou, *Chem. Commun.* **2004**, 520-521.

[13] K. Barthelet, K. Adil, F. Millange, C. Serre, D. Riou, G. Férey, *J. Mater. Chem.* **2003**, *13*, 2208-2212.

[14] A. Phan, A. U. Czaja, F. Gándara, C. B. Knobler, O. M. Yaghi, *Inorg. Chem.* **2011**, *50*, 7388-7390.

[15] Z. Lu, H. G. W. Godfrey, I. da Silva, Y. Cheng, M. Savage, F. Tuna, E. J. L. McInnes, S. J. Teat, K. J. Gagnon, M. D. Frogley, P. Manuel, S. Rudić, A. J. Ramirez-Cuesta, T. L. Easun, S. Yang, M. Schröder, *Nat. Commun.* **2017**, *8*, 14212.

[16] K. B. Idrees, Z. Li, H. Xie, K. O. Kirlikovali, M. Kazem-Rostami, X. Wang, X. Wang, T.-Y. Tai, T. Islamoglu, J. F. Stoddart, R. Q. Snurr, O. K. Farha, *J. Am. Chem. Soc.* **2022**, *144*, 12212-12218.

[17] A. Lieb, H. Leclerc, T. Devic, C. Serre, I. Margiolaki, F. Mahjoubi, J. S. Lee, A. Vimont, M. Daturi, J.-S. Chang, *Microporous Mesoporous Mater.* **2012**, *157*, 18-23.

[18] F. Carson, J. Su, A. E. Platero-Prats, W. Wan, Y. Yun, L. Samain, X. Zou, *Cryst. Growth Des.* **2013**, *13*, 5036-5044.

[19] D. Ma, P. Li, X. Duan, J. Li, P. Shao, Z. Lang, L. Bao, Y. Zhang, Z. Lin, B. Wang, *Angew. Chem. Int. Ed.* **2020**, *59*, 3905-3909.

[20] C. Volkringer, D. Popov, T. Loiseau, G. Férey, M. Burghammer, C. Riekel, M. Haouas, F. Taulelle, *Chem. Mater.* **2009**, *21*, 5695-5697.

[21] G. Férey, C. Mellot-Draznieks, C. Serre, F. Millange, J. Dutour, S. Surblé, I. Margiolaki, *Science* **2005**, *309*, 2040-2042.

[22] D. Reinares-Fisac, L. M. Aguirre-Díaz, M. Iglesias, N. Snejko, E. Gutiérrez-Puebla, M. Á. Monge, F. Gándara, *J. Am. Chem. Soc.* **2016**, *138*, 9089-9092.

[23] S. Yang, J. Sun, A. J. Ramirez-Cuesta, S. K. Callear, W. I. F. David, D. P. Anderson, R. Newby, A. J. Blake, J. E. Parker, C. C. Tang, M. Schröder, *Nat. Chem.* **2012**, *4*, 887-894.

[24] K. Barthelet, D. Riou, G. Férey, *Chem. Commun.* **2002**, 1492-1493.

[25] J. Zhu, X. Chen, A. Q. Thang, F.-L. Li, D. Chen, H. Geng, X. Rui, Q. Yan, *SmartMat* **2022**, *3*, 384-416.

[26] X. Zhao, X. Bu, Q.-G. Zhai, H. Tran, P. Feng, *J. Am. Chem. Soc.* **2015**, *137*, 1396-1399.

[27] X. Zhao, X. Bu, E. T. Nguyen, Q.-G. Zhai, C. Mao, P. Feng, *J. Am. Chem. Soc.* **2016**, *138*, 15102-15105.

[28] S.-T. Zheng, X. Zhao, S. Lau, A. Fuhr, P. Feng, X. Bu, *J. Am. Chem. Soc.* **2013**, *135*, 10270-10273.

[29] S. Surblé, C. Serre, C. Mellot-Draznieks, F. Millange, G. Férey, *Chem. Commun.* **2006**, 284-286.

[30] A. C. Sudik, A. P. Côté, O. M. Yaghi, *Inorg. Chem.* **2005**, *44*, 2998-3000.

[31] Q.-G. Zhai, X. Bu, C. Mao, X. Zhao, L. Daemen, Y. Cheng, A. J. Ramirez-Cuesta, P. Feng, *Nat. Commun.* **2016**, *7*, 13645.

[32] H. Yang, Y. Wang, R. Krishna, X. Jia, Y. Wang, A. N. Hong, C. Dang, H. E. Castillo, X. Bu, P. Feng, *J. Am. Chem. Soc.* **2020**, *142*, 2222-2227.

[33] Y. Chen, H. Yang, W. Wang, X. Li, Y. Wang, A. N. Hong, X. Bu, P. Feng, *Small* **2023**, *19*, 2303540.

[34] Q.-G. Zhai, X. Bu, X. Zhao, D.-S. Li, P. Feng, *Acc. Chem. Res.* **2017**, *50*, 407-417.

[35] Y. Wang, X. Zhao, H. Yang, X. Bu, Y. Wang, X. Jia, J. Li, P. Feng, *Angew. Chem. Int. Ed.* **2019**, *58*, 6316-6320.

[36] Y. Wang, X. Jia, H. Yang, Y. Wang, X. Chen, A. N. Hong, J. Li, X. Bu, P. Feng, *Angew. Chem. Int. Ed.* **2020**, *59*, 19027-19030.

[37] A. N. Hong, H. Yang, T. Li, Y. Wang, Y. Wang, X. Jia, A. Zhou, E. Kusumoputro, J. Li, X. Bu, P. Feng, *ACS Appl. Mater. Interfaces* **2021**, *13*, 52160-52166.

[38] H. Yang, F. Peng, A. N. Hong, Y. Wang, X. Bu, P. Feng, *J. Am. Chem. Soc.* **2021**, *143*, 14470-14474.

[39] A. N. Hong, E. Kusumoputro, Y. Wang, H. Yang, Y. Chen, X. Bu, P. Feng, *Angew. Chem. Int. Ed.* **2022**, *61*, e202116064.

[40] A. N. Hong, H. Yang, X. Bu, P. Feng, *EnergyChem* **2022**, *4*, 100080.

[41] H. Yang, Y. Chen, C. Dang, A. N. Hong, P. Feng, X. Bu, *J. Am. Chem. Soc.* **2022**, *144*, 20221-20226.

[42] A. N. Hong, Y. Wang, Y. Chen, H. Yang, E. Kusumoputro, X. Bu, P. Feng, *Chem. Eur. J.* **2023**, *29*, e202203547.

[43] Y. Xiao, Y. Chen, A. N. Hong, X. Bu, P. Feng, *Angew. Chem. Int. Ed.* **2023**, *62*, e202300721.

[44] Y. Xiao, Y. Chen, W. Wang, H. Yang, A. N. Hong, X. Bu, P. Feng, *J. Am. Chem. Soc.* **2023**, *145*, 10980-10986.

[45] Y. Xiao, A. N. Hong, Y. Chen, H. Yang, Y. Wang, X. Bu, P. Feng, *Small* **2023**, *19*, 2205119.

[46] W. Wang, H. Yang, Y. Chen, X. Bu, P. Feng, *J. Am. Chem. Soc.* **2023**, *145*, 17551-17556.

[47] H.-R. Yang, W.-Y. Chen, D.-M. Chen, Y.-P. Zheng, S.-M. Fang, *J. Solid State Chem.* **2020**, *291*, 121658.

[48] Y. Ye, Z. Ma, R.-B. Lin, R. Krishna, W. Zhou, Q. Lin, Z. Zhang, S. Xiang, B. Chen, *J. Am. Chem. Soc.* **2019**, *141*, 4130-4136.

[49] J.-W. Wang, S.-C. Fan, H.-P. Li, X. Bu, Y.-Y. Xue, Q.-G. Zhai, *Angew. Chem. Int. Ed.* **2023**, *62*, e202217839.

[50] T. Xu, Z. Jiang, P. Liu, H. Chen, X. Lan, D. Chen, L. Li, Y. He, *ACS Applied Nano Materials* **2020**, *3*, 2911-2919.

[51] L. Fan, L. Yue, W. Sun, X. Wang, P. Zhou, Y. Zhang, Y. He, *ACS Appl. Mater. Interfaces* **2021**, *13*, 40788-40797.

[52] R.-B. Lin, L. Li, H. Wu, H. Arman, B. Li, R.-G. Lin, W. Zhou, B. Chen, *J. Am. Chem. Soc.* **2017**, *139*, 8022-8028.

[53] J. Pei, K. Shao, J.-X. Wang, H.-M. Wen, Y. Yang, Y. Cui, R. Krishna, B. Li, G. Qian, *Adv. Mater.* **2020**, *32*, 1908275.

[54] Y.-P. Li, Y.-N. Zhao, S.-N. Li, D.-Q. Yuan, Y.-C. Jiang, X. Bu, M.-C. Hu, Q.-G. Zhai, *Adv. Sci.* **2021**, *8*, 2003141.

[55] X. Duan, Q. Zhang, J. Cai, Y. Yang, Y. Cui, Y. He, C. Wu, R. Krishna, B. Chen, G. Qian, *J. Mater. Chem. A* **2014**, *2*, 2628-2633.

[56] Z. Bao, S. Alnemrat, L. Yu, I. Vasiliev, Q. Ren, X. Lu, S. Deng, *Langmuir* **2011**, *27*, 13554-13562.

[57] C. Campbell, C. A. Ferreiro-Rangel, M. Fischer, J. R. B. Gomes, M. Jorge, *J. Phys. Chem. C* **2017**, *121*, 441-458.

[58] K. Liu, D. Ma, B. Li, Y. Li, K. Yao, Z. Zhang, Y. Han, Z. Shi, *J. Mater. Chem. A* **2014**, *2*, 15823-15828.

[59] X. Duan, H. Wang, Z. Ji, Y. Cui, Y. Yang, G. Qian, *Mater. Lett.* **2017**, *196*, 112-114.

[60] Y. He, Z. Zhang, S. Xiang, F. R. Fronczek, R. Krishna, B. Chen, *Chem. Eur. J.* **2012**, *18*, 613-619.

[61] Y. He, Z. Zhang, S. Xiang, F. R. Fronczek, R. Krishna, B. Chen, *Chem. Commun.* **2012**, *48*, 6493-6495.

[62] P. Zhou, L. Yue, X. Wang, L. Fan, D.-L. Chen, Y. He, *ACS Appl. Mater. Interfaces* **2021**, *13*, 54059-54068.

[63] Y. Chen, Z. Wu, L. Fan, R. Krishna, H. Huang, Y. Wang, Q. Xiong, J. Li, L. Li, *Engineering* **2024**.

[64] W. Liang, F. Xu, X. Zhou, J. Xiao, Q. Xia, Y. Li, Z. Li, *Chem. Eng. Sci.* **2016**, *148*, 275-281.

[65] R.-B. Lin, H. Wu, L. Li, X.-L. Tang, Z. Li, J. Gao, H. Cui, W. Zhou, B. Chen, *J. Am. Chem. Soc.* **2018**, *140*, 12940-12946.

[66] P.-Q. Liao, W.-X. Zhang, J.-P. Zhang, X.-M. Chen, *Nat. Commun.* **2015**, *6*, 8697.

[67] U. Böhme, B. Barth, C. Paula, A. Kuhnt, W. Schwieger, A. Mundstock, J. Caro, M. Hartmann, *Langmuir* **2013**, *29*, 8592-8600.

[68] C. He, Y. Wang, Y. Chen, X. Wang, J. Yang, L. Li, J. Li, *Chem. Eng. J.* **2021**, *403*, 126428.

[69] A.-R. Kim, T.-U. Yoon, E.-J. Kim, J. W. Yoon, S.-Y. Kim, J. W. Yoon, Y. K. Hwang, J.-S. Chang, Y.-S. Bae, *Chem. Eng. J.* **2018**, *331*, 777-784.

[70] W. Fan, X. Wang, X. Zhang, X. Liu, Y. Wang, Z. Kang, F. Dai, B. Xu, R. Wang, D. Sun, *ACS Cent. Sci.* **2019**, *5*, 1261-1268.

[71] P. Huang, C. Chen, Z. Hong, J. Pang, M. Wu, F. Jiang, M. Hong, *Inorg. Chem.* **2019**, *58*, 11983-11987.

[72] Y. Wang, T. Li, L. Li, R.-B. Lin, X. Jia, Z. Chang, H.-M. Wen, X.-M. Chen, J. Li, *Adv. Mater.* **2023**, *35*, 2207955.

TOC

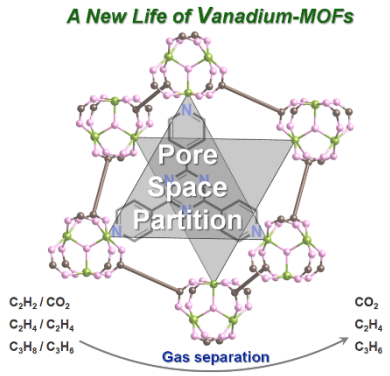
A New Life of Vanadium-MOFs
Pore
Space
Partition
C_2H_2 / CO_2
C_2H_4 / C_2H_4
C_3H_8 / C_3H_6
Gas separation
CO_2
C_2H_4
C_3H_6